Development and Characterisation of Asbestos-Free Ceramic–Glass Fibre Reinforced Phenolic Brake Linings for Tricycle Drum Braking Systems in Nigeria

[1]Adeniyi O. Adesina, [2]Oyelaran. A. M, [3]Kazeem A. Bello, [4]Lukman A. Animashaun, [5]Olaiya A. Kabiru, [6]Adebola M. Oghene, and [7]Ridwan A. Oyetunde

[1,6,7]Department of Mechanical Engineering, Yaba College of Technology, Yaba, Lagos, Nigeria

[2,3]Department of Mechanical Engineering, Federal University, Oye-Ekiti, Ekiti State, Nigeria

[4,5]Lagos State University of Science and Technology, Ikorodu, Lagos, Nigeria

oluwole.adesina@yabatech.edu.ng | olatunde.oyelaran@fuoye.edu.ng | kazeem.bello@fuoye.edu.ng | animashaun.l@lasustech.edu.ng | olaiya.k@lasustech.edu.ng | adebola.oghene@yabatech.edu.ng | ridwan.oyetunde@yabatech.edu.ng

Received: 30-JULY-2026; Reviewed: 16-SEPT-2026; Accepted: 25-SEPT-2026

https://dx.doi.org/10.46792/fuoyejet.v11i3.1633

ORIGINAL RESEARCH

Abstract— Commercial tricycles carry much of Nigeria's urban passenger traffic, yet their drum brake linings are almost entirely imported and poorly matched to a duty cycle of overloading, stop–start braking and degraded road surfaces. Three asbestos-free friction composites were developed and characterised against a commercial lining. Kaolin-derived ceramic fibre was set at 20, 25 and 30 wt% (Samples A, B and C) with E-glass fibre, phenolic and vinylester resins, polypropylene and copper–iron powder. Binder and metal powder fractions varied alongside the fibre, so the series compares three candidate formulations rather than isolating fibre content. Specimens were compression moulded at a nominal 50 MPa and 160 °C for 10 min and post-cured at 175 °C for 7 h. Bulk density, apparent porosity, water absorption, Brinell hardness, wear rate, compressive strength and impact energy were measured. Sample A returned the best overall profile: lowest apparent porosity (14.29%), lowest water absorption (0.44%), lowest wear rate (0.273 g/min) and highest compressive strength (116.20 N/mm²), for a composite desirability of 0.571 against 0.454 and 0.424 for Samples C and B. Analysis of variance confirmed the strength differences as significant, $F(2, 3) = 24.9$, $p = 0.014$, though the spread is only 3.1%. Hardness rose from 121 to 143 HB as strength fell, an ordering tentatively attributed to binder starvation at higher reinforcement loadings. Strength, porosity and water absorption fall within ranges reported for published asbestos-free linings; bulk density alone falls short. Sample A is proposed as the preferred formulation, subject to friction, thermal and microstructural testing.

Keywords— asbestos-free brake lining, binder starvation, ceramic fibre, compression moulding, drum brake, phenolic composite

1 Introduction

The drum brake system has the friction interface as the main component, which is the brake lining. The wheel cylinder pushes it against the rotating drum, generating heat by controlled sliding contact with the drum, while the kinetic energy of the vehicle is transferred. The material properties are thus directly related to stopping distance, thermal stability and, ultimately, occupant safety. Friction materials were dominated by asbestos in the twentieth century, because it had many desirable properties, including thermal resistance, mechanical strength and low cost. That changed once asbestos was classified as carcinogenic to humans by the International Agency for Research on Cancer (2012), which drove a shift to non-asbestos organic, semi-metallic and ceramic formulations (Bijwe, 1997; Kumar & Kumaran, 2019). The transition has been uneven in Nigeria. Commercial tricycles (Keke NAPEP or Maruwa) carry a substantial share of urban passenger movement, and the replacement lining market for them is served largely by imported product. Price pressure sustains a large market for low-grade parts, and the operating conditions are severe: tricycles are routinely overloaded, brake frequently in dense traffic and operate on rough or damaged surfaces. Lining formulations developed for temperate, well-surfaced markets are poorly matched to this duty cycle, and premature wear, brake fade and failure are commonly observed. Brake-system failure remains among the recorded causes of road traffic crashes in Nigeria (Federal Road Safety Corps, 2021).

1.1 Related Work on Asbestos-Free Friction Composites

Research on asbestos substitutes in West Africa has concentrated on agricultural residues. Palm kernel shell (Ibhadode & Dagwa, 2008; Adetunji et al., 2022), palm kernel fibre (Ikpambese et al., 2016), banana peel (Idris et al., 2015), coconut shell (Ocheri et al., 2024) and Costus afer stem (Ngwaba & Aikhuele, 2023) have all been reported as viable reinforcements, generally at low cost and with acceptable friction behaviour. These reinforcements share a common ceiling: lignocellulosic fillers lose thermal stability well below the interface temperatures reached in sustained braking (Bashir et al., 2019). Their reported performance is therefore established under mechanical and physical testing rather than under thermal loading, and the literature seldom says so explicitly. Ceramic fibre occupies the opposite position. It is chemically inert, sustains a stable friction coefficient over a wide temperature range and generates comparatively low dust in service (Hee & Filip, 2005; Mutlu et al., 2005). Its drawbacks are cost and import dependence, which have largely confined it to high-value

Corresponding Author: oluwole.adesina@yabatech.edu.ng

Section C- MECHANICAL/MECHATRONICS ENGINEERING & RELATED SCIENCES

Can be cited as:

Adesina A.O., Oyelaran A.M., Bello K.A., Animashaun L.A., Kabiru O.A., Oghene A.M. and Oyetunde R.A. (2026). Development and Characterisation of Asbestos-Free Ceramic–Glass Fibre Reinforced Phenolic Brake Linings for Tricycle Drum Braking Systems in Nigeria (2026). FUOYE Journal of Engineering and Technology (FUOYE**JET**), **11(1), 490-500.**

https://dx.doi.org/10.46792/fuoyejet.v11i3.1633

© 2026 The Author(s). Published by Faculty of Engineering, Federal University Oye-Ekiti.
This is an open access article under the CC BY NC license. (https://creativecommons.org/licenses/by-nc/4.0/)

applications. Blending ceramic fibre with lower-cost E-glass fibre and metallic fillers offers a route to retaining thermal performance at moderate cost (Singh et al., 2020), and metal powders additionally provide heat dissipation paths that limit hot-spot formation (Jang et al., 2004; Thiyagarajan et al., 2016).

The evidence base for ceramic and hybrid systems is, however, stronger on thermal behaviour than on formulation. Hee and Filip (2005) demonstrated that ceramic-enhanced phenolic linings hold a stable friction coefficient at interface temperatures well above the degradation range of organic reinforcements, and Mutlu et al. (2005) reported comparable gains for ceramic-additive linings; in both cases several constituents were varied simultaneously and no single-variable loading study was reported. Formulation reviews reach the same conclusion from the opposite direction: Bijwe (1997) and Kumar and Kumaran (2019) both find that published friction formulations are rarely comparable, because fibre content, binder fraction, moulding pressure and cure schedule differ between studies. The consequence is that the reported property ranges for ceramic friction composites are wide and cannot be attributed to composition alone. Hybridisation is the usual response to the cost of ceramic fibre, and here the limitation is the same. Singh et al. (2020) combined chemically treated natural and synthetic fibres and obtained useful mechanical properties at reduced cost, and Thiyagarajan et al. (2016) showed that metallic fillers raise thermal conductivity and suppress hot-spot formation in non-asbestos composites. Neither study varied the ceramic fraction systematically against a fixed process, so the trade-off between reinforcement content and binder availability is described qualitatively rather than quantified.

What the wider composites literature does establish is that reinforcement content has an optimum rather than a monotonic benefit, and that the optimum is set by the binder-to-reinforcement ratio rather than by fibre content alone. Ammar et al. (2023), reviewing fibre-reinforced brake composites, report that mechanical and tribological properties improve with reinforcement content up to a point and deteriorate beyond it: below the optimum ratio there is too little reinforcement to strengthen the matrix, and above it the fibres require more binder than is available to bind them together. The same pattern is reported outside friction materials: Ambali et al. (2023) found that reinforcement particles in stir-cast aluminium composites were well distributed up to 10–15 wt% but agglomerated again at 20 wt%, with a corresponding fall in mechanical properties, and identified insufficient wetting of the reinforcement as the cause. A comparable dependence of hardness on reinforcement content has been reported for other locally developed composite systems (Asafa et al., 2020). Processing sensitivity compounds this: Ammar et al. (2023) further report that the compaction load applied during manufacture governs void content and hence the mechanical properties obtained, and reinforcement–matrix wetting is itself process-dependent (Ambali et al., 2022).

1.2 Research Gap, Contribution and Objectives

Three gaps follow from the foregoing. First, no published study steps ceramic fibre content through a defined range in a kaolin-derived ceramic–E-glass–phenolic lining while holding the fabrication route fixed, so reported property variations cannot be separated from processing differences between laboratories. Second, the tricycle drum brake, a high-duty, low-cost application carrying a large share of West African urban mobility, is essentially absent from the friction materials literature, which is written around passenger-car service. Third, asbestos-free work in the region reports agricultural reinforcements almost exclusively, whose thermal ceiling lies below braking interface temperatures.

This work is distinct from the studies cited above in four specific respects. First, the reinforcement is kaolin-derived ceramic fibre hybridised with E-glass rather than an agricultural residue. Second, the three formulations were produced in a single fabrication campaign under one moulding and cure route, so the comparison between them is not confounded by process differences between laboratories, even though it does not isolate ceramic fibre as a single variable. Third, seven physical and mechanical properties are reported against a commercial lining tested in the same session, rather than against published values alone. Fourth, the target application is the Nigerian tricycle drum brake duty cycle. The formulations, the measured data and the findings reported here have not been published elsewhere in whole or in part.

The objectives are: (i) to quantify how seven physical and mechanical properties vary across the three formulations; (ii) to identify the mechanism most consistent with the observed ordering; (iii) to benchmark the results against published asbestos-free linings and recognised specification values; and (iv) to identify a preferred formulation to carry forward into tribological and thermal qualification for tricycle drum service.

2 Materials and Methods

The linings developed in this work were designed for the tricycle drum brake assembly shown in Fig. 1, which locates the lining and shoe within the drum, wheel cylinder and return-spring arrangement.

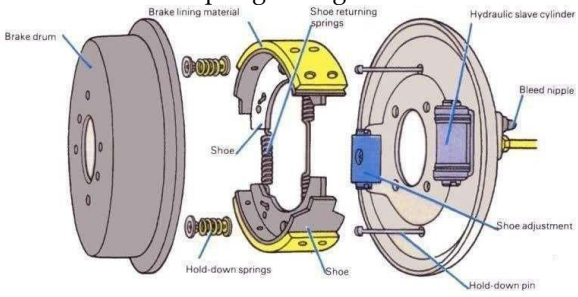

Fig. 1. Exploded view of a tricycle drum brake assembly for which the linings were developed.

2.1 Constituent Materials

Kaolin-derived ceramic fibre was the primary reinforcement, selected for thermal stability above 1000 °C, low thermal conductivity and chemical inertness. E-glass fibre provided tensile reinforcement and impact toughness at moderate cost. Phenolic resin served as the principal binder, chosen for thermal stability, adhesion to inorganic fillers and established use in commercial friction materials (Kumar & Kumaran, 2019). Vinylester resin blended with polypropylene was added as a secondary matrix to improve toughness and corrosion

© 2026 The Author(s). Published by Faculty of Engineering, Federal University Oye-Ekiti.
This is an open access article under the CC BY NC license. (https://creativecommons.org/licenses/by-nc/4.0/)

http://.doi.org/10.46792/fuoyejet.v11i3.1633 engineering.fuoye.edu.ng/journal

resistance. Polypropylene is a thermoplastic melting near 165 °C, below the interface temperatures reached in sustained braking, so it is present as a minor toughening phase whose behaviour at service temperature was not established in this work. Copper–iron metal powder was included to raise thermal conductivity and assist heat dissipation during braking (Thiyagarajan et al., 2016). The constituents are shown in Fig. 2.

(a) Ceramic fibre (b) Glass fibre

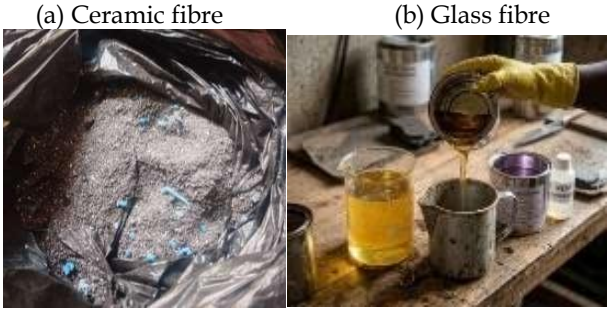

(c) Metal powder (d) Vinylester resin

(e) Polypropylene

Fig. 2. Constituent materials.

2.2 FORMULATIONS

Three formulations were prepared (Table 1). Ceramic fibre was stepped through 20, 25 and 30 wt%. This range was selected from published practice rather than arbitrarily. Reinforcement content in fibre-reinforced phenolic friction composites is reported to raise hardness to an optimum and then reverse as the binder available to wet each fibre becomes insufficient (Ammar et al., 2023; Ibhadode & Dagwa, 2008; Ambali et al., 2023), and organic polymeric friction materials typically carry 30–40 wt% resin (Ammar et al., 2023). A lower bound of 20 wt% was set so that the thermal contribution of the ceramic phase would be material, and an upper bound of 30 wt% so that the phenolic fraction would not fall below the level at which commercial formulations remain processable. The three levels therefore bracket the reported optimum rather than merely sampling a convenient range.Glass fibre was held at 5 wt% throughout. Phenolic binder was held at 50 wt% in Samples A and B and reduced to 45 wt% in Sample C to accommodate the highest fibre loading. Metal powder was reduced from 20 wt% in Sample A to 10 wt% in B and C, with vinylester and polypropylene taking up the balance. The resulting binder-to-reinforcement ratio falls from 2.00 in Sample A to 1.67 in B and 1.29 in C (Table 1), and this ratio rather than fibre content alone is the quantity against which the results are interpreted.

Metal powder, phenolic resin and the vinylester–polypropylene fraction were varied alongside ceramic fibre, so the property differences reported represent the combined response of the three formulations as prepared. Each trend observed with rising fibre content is equally consistent with the concurrent fall in binder-to-reinforcement ratio and, for Samples B and C, with the reduced metal powder content. The series is accordingly treated throughout as a comparison of three candidate formulations. A design isolating ceramic fibre as the sole independent variable, with binder and metallic filler held constant and an inert filler taking up the balance, is identified among the priorities for further work.

TABLE 1. COMPOSITION OF THE THREE FORMULATIONS (WT%)

Constituent	A	B	C
Ceramic fibre	20	25	30
Glass fibre	5	5	5
Phenolic resin	50	50	45
Vinylester + PP	5	10	10
Metal powder	20	10	10
Total	100	100	100
Binder : reinforcement ratio	2.00	1.67	1.29

2.3 FABRICATION

All constituents were oven-dried to remove adsorbed moisture and weighed to formulation on a digital balance. Blending was performed manually in a metal vessel until the mixture was visually homogeneous, ensuring uniform distribution of ceramic particles, fibreglass and binder throughout the matrix. The blend was charged into a cleaned mild-steel mould shaped to the tricycle drum shoe profile and consolidated in a hydraulic compression press at a nominal moulding pressure of 50 MPa, with the platens held at 160 °C for a dwell time of 10 min to initiate cross-linking of the phenolic binder. Post-curing was completed in the workshop hot-air oven at 175 °C for 7 h, providing the thermal environment required for full polymerisation of the resin and expulsion of residual moisture, and developing the hardness and wear resistance of the finished lining.

These conditions were applied to all three formulations. The series was produced in a single fabrication campaign, on the same equipment and to the same schedule, so the three formulations share a common processing history and the comparison between them rests on composition.

(a) Steel mould (b) Finished linings

Fig. 3. Fabrication sequence: manual blending, compression moulding, oven curing and the finished brake linings bonded to steel backing plates.

After curing, moulds were cooled gradually in still air to ambient temperature to avoid the residual stresses and surface cracking associated with rapid quenching. The cured friction material was bonded to a steel backing plate using a high-temperature adhesive under uniform press load, then trimmed, surface-ground to uniform

© 2026 The Author(s). Published by Faculty of Engineering, Federal University Oye-Ekiti.
This is an open access article under the CC BY NC license. (https://creativecommons.org/licenses/by-nc/4.0/)

http://.doi.org/10.46792/fuoyejet.v11i3.1633 engineering.fuoye.edu.ng/journal

thickness and inspected dimensionally. The steel mould and the finished linings are shown in Figure 3.

2.4 Characterisation and Governing Equations

2.4.1 Bulk density

Each specimen was oven-dried and weighed to obtain the dry mass W_1. Bulk density was determined by the Archimedes method on the same specimens used for the apparent porosity determination, from the saturated mass W_2 and the mass suspended in water W_3:

$$\rho_b = \frac{W_1}{W_2 - W_3} \quad (1)$$

Specimen volumes were also determined independently by direct water displacement. Those values were not adopted: for the three developed formulations they disagreed with the Archimedes volumes by up to 60%, and they implied bulk densities above the pore-free density estimated for these compositions by rule of mixtures, which is not physically admissible. The two determinations agreed for the commercial reference. Because the Archimedes route uses the same specimens and the same weighings as the porosity determination, it is adopted throughout.

2.4.2 Apparent porosity

Specimens were dried and weighed (W_1), boiled in water for 2 h, surface-dried and weighed again (W_2), then weighed while suspended in water (W_3). Open pore fraction follows

$$P_a = \frac{W_2 - W_1}{W_2 - W_3} \times 100\% \quad (2)$$

2.4.3 Water absorption

Specimens were oven-dried, weighed, immersed in distilled water for 24 h at room temperature, surface-wiped and reweighed. Moisture uptake follows ASTM D570 practice (ASTM International, 2018a):

$$W_a = \frac{W_2 - W_1}{W_1} \times 100\% \quad (3)$$

2.4.4 Brinell hardness

Hardness was measured on a GUNT WP 300 materials testing apparatus following ASTM E10 (ASTM International, 2018b), using a D = 10 mm ball indenter under an applied load F = 9.8 kN, with the indentation diameter d measured optically:

$$HB = \frac{0.102 \times 2F}{\pi D\left(D - \sqrt{D^2 - d^2}\right)} \quad (4)$$

The 9.8 kN load with a 10 mm ball is the $F/D^2 = 10$ condition specified in ASTM E10 for metallic materials. It is applied here to a polymer-matrix composite, so the resulting Brinell numbers are used only to rank materials indented under identical conditions and are not directly comparable with hardness data obtained on scales intended for friction composites, such as Rockwell L or M or Shore D.

2.4.5 Wear rate

Specimens were weighed, subjected to frictional contact against a rotating counterface for a fixed interval of t = 3 min, and reweighed. All four materials were tested consecutively on the same rig under identical settings. Gravimetric wear rate follows (5) and is reported as a comparison between the materials tested in this session rather than as a specific wear rate in mm³/N·m.

$$\dot{W} = \frac{W_1 - W_2}{t} \quad (5)$$

Wear rates are reported as a comparison between the materials tested in this session, which were run consecutively on the same rig under identical settings, rather than as a specific wear rate in mm³/N·m.

2.4.6 Compressive strength

Uniaxial compression was performed on a Testometric universal testing machine using cylindrical specimens of D = 12.7 mm and H = 25.4 mm, a 2:1 aspect ratio adopted to suppress geometric buckling. Peak stress follows

$$\sigma_c = \frac{F_{max}}{A_0}, \quad A_0 = \frac{\pi D^2}{4} \quad (6)$$

with engineering strain from platen displacement ΔH:

$$\varepsilon = \frac{\Delta H}{H_0} \times 100\% \quad (7)$$

Two replicate runs were performed per formulation on separate specimens.

2.4.7 Impact energy

Impact energy was measured on a standard pendulum impact tester as the energy absorbed to fracture. Because specimen cross-section was not standardised against a notched-bar geometry, the absorbed energies are reported in joules and are used only for comparison between the materials tested here.

2.4.8 Composite desirability

To rank formulations across the property set, each property was min–max normalised over the three samples, with properties for which lower values are preferable inverted, and combined with equal weighting:

$$D = \frac{1}{n}\sum d_i, \quad d_i = \frac{x_i - x_{min}}{x_{max} - x_{min}} \quad (8)$$

Equal weighting is adopted deliberately. Absent dynamometer data no defensible application-specific weighting exists, and equal weighting keeps the ranking transparent and reproducible.

2.5 Statistical Analysis

Compressive strength was measured on two specimens per formulation, so means are reported with the sample standard deviation and the two-run range. Differences between formulations were tested by one-way analysis of variance on the six compression runs, with Fisher's least significant difference used for pairwise separation at α = 0.05.

Bulk density, apparent porosity, water absorption, Brinell hardness, wear rate and impact energy were determined once per material. The comparisons reported for those properties are therefore descriptive, and the corresponding differences between formulations are presented as an ordering rather than as tested effects.

Pearson correlation coefficients between properties are computed across the three formulations. With n = 3 these carry one degree of freedom, and the associated p-value is reported alongside every coefficient so that its weight can be judged. None reaches significance at α = 0.05. The coefficients are used in this paper as a compact description of ordering across three formulations and not as evidence of an established relationship.

3 Results

The prepared specimens are shown in Figure 4. All were produced to the cylindrical geometry specified above, 12.7 mm in diameter and 25.4 mm in height, and were inspected dimensionally before testing. Specimens of all three formulations emerged from the mould intact, with clean edges and no visible delamination or surface cracking after curing and controlled cooling, confirming that the moulding and cure schedule produced coherent bodies in every case. The results that follow were

© 2026 The Author(s). Published by Faculty of Engineering, Federal University Oye-Ekiti.
This is an open access article under the CC BY NC license. (https://creativecommons.org/licenses/by-nc/4.0/)

http://.doi.org/10.46792/fuoyejet.v11i3.1633 engineering.fuoye.edu.ng/journal

obtained on specimens of this common geometry, so the comparisons between formulations are not confounded by differences in specimen form.

Fig. 4. Prepared compression specimens of the three formulations.

3.1 Bulk Density

Bulk density measures the compactness of the lining and its capacity to carry mechanical load. Table 2 and Figure 5 give the results. Sample A returned 1.29 g/cm³, Sample B 1.54 g/cm³ and Sample C 1.36 g/cm³, against 2.18 g/cm³ for the commercial reference.

Density does not vary monotonically with ceramic fibre loading. Sample B is the densest of the three at 1.54 g/cm³ and Sample A the least dense at 1.29 g/cm³, a spread of 20% that does not track the reinforcement content. All three developed linings are substantially less dense than the commercial reference and fall below the 1.8–2.5 g/cm³ range reported for non-asbestos organic linings (Kumar & Kumaran, 2019), whereas the commercial reference sits within it. Low bulk density combined with an open porosity of only 14–17% indicates that a proportion of the void volume is closed rather than interconnected, which reflects the degree of consolidation achieved during moulding. The absence of a monotonic relationship with fibre loading points to the same origin: compaction governs this property more strongly than composition does. The point is developed in the discussion of consolidation below.

TABLE 2: BULK DENSITY AND APPARENT POROSITY RESULTS

Sample	W_1 (g)	W_2 (g)	W_3 (g)	ρb (g/cm³)	Pa (%)
Sample A	45	50	15	1.29	14.29
Sample B	54	60	25	1.54	17.14
Sample C	45	50	17	1.36	15.15
Commercial	48	52	30	2.18	18.18

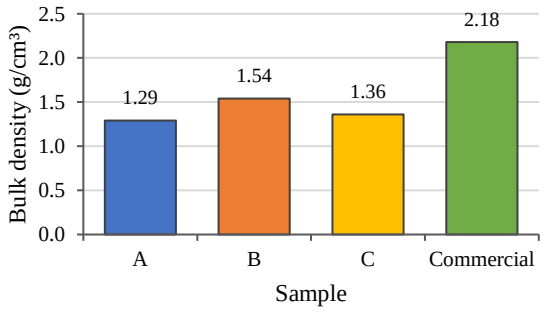

Fig. 5. Bulk density of the three formulations against the commercial reference, determined by the Archimedes method from the data of Table 2.

3.2 Apparent Porosity

Apparent porosity quantifies the open pore fraction, which governs moisture ingress, mechanical strength and wear resistance. Results appear in Table 2 and Figure 6.

Sample A returned the lowest porosity at 14.29%, indicating the best interparticle bonding of the three. Sample C followed at 15.15% and Sample B recorded the highest at 17.14%. The commercial lining measured 18.18%, so every developed formulation is less porous than the reference. The three developed linings lie within the range reported for non-asbestos organic linings, in which porosity falls as reinforcement content rises (Ammar et al., 2023), with the commercial reference marginally above.

The elevated value for Sample B is consistent with void volume introduced during mixing and compaction. That Sample B is not the highest-fibre formulation yet records the highest porosity indicates that compaction, rather than composition alone, governs the pore structure, a point developed below.

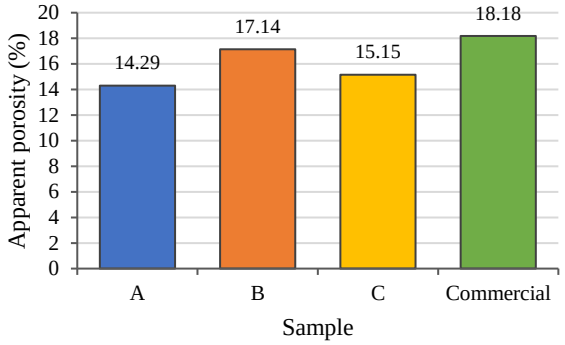

Fig. 6. Apparent porosity of the three formulations against the commercial reference. All three developed linings are less porous than the reference.

3.3 Water Absorption

Moisture uptake affects wet braking performance, interfacial bonding and long-term durability, and low values are required. Table 3 and Figure 7 give the results. Sample A absorbed 0.44%, Sample B 1.85% and Sample C 2.22%, against 2.50% for the commercial lining. Absorption rises monotonically with ceramic fibre loading, and the ordering matches the compressive strength ordering inversely, consistent with a common underlying cause in the fibre–matrix interface.

TABLE 3: WATER ABSORPTION RESULTS

Sample	W_1 (g)	W_2 (g)	Wa (%)
Sample A	45	45.2	0.44
Sample B	54	55	1.85
Sample C	45	46	2.22
Commercial	48	49.2	2.50

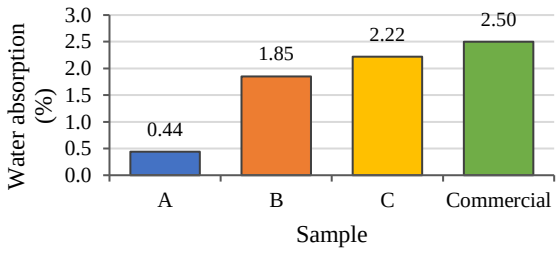

Fig. 7. Water absorption of the three formulations after 24 h immersion, against the commercial reference.

Every developed formulation absorbs less moisture than the commercial reference. Sample A, at 0.44%, is well below the 1.2% reported for a Costus afer composite under comparable ASTM D570 practice (Ngwaba & Aikhuele, 2023), while Samples B and C exceed that figure by roughly a factor of two, consistent with the rising void content that accompanies higher fibre loading.

© 2026 The Author(s). Published by Faculty of Engineering, Federal University Oye-Ekiti.
This is an open access article under the CC BY NC license. (https://creativecommons.org/licenses/by-nc/4.0/)

http://.doi.org/10.46792/fuoyejet.v11i3.1633 engineering.fuoye.edu.ng/journal

3.4 Brinell Hardness

Hardness governs resistance to indentation, surface deformation and abrasive wear. Measurements were made under a 9.8 kN load with a 10 mm ball indenter; the values reproduce equation (4) from the recorded indentation diameters (Table 4, Fig. 8).

Hardness rises monotonically with ceramic fibre loading: 121 HB for Sample A, 129 HB for Sample B and 143 HB for Sample C, an 18.2% increase across the series. The commercial reference measured 178 HB and is harder than all three developed formulations, by 20% against Sample C and 32% against Sample A. The increase across the series follows directly from the rising area fraction of hard ceramic particles encountered by the indenter, while the shortfall against the commercial lining indicates a higher abrasive or metallic content in the reference material. All four materials were indented under identical conditions, so the ranking is on a like-for-like basis; comparison with published hardness values is subject to the scale considerations set out in the methods, and the Brinell numbers are not consistent with the measured compressive strengths in the way that would be expected for a metal.

TABLE 4: BRINELL HARDNESS RESULTS

Sample	d (mm)	HB
Sample A	3.20	121
Sample B	3.10	129
Sample C	2.95	143
Commercial	2.65	178

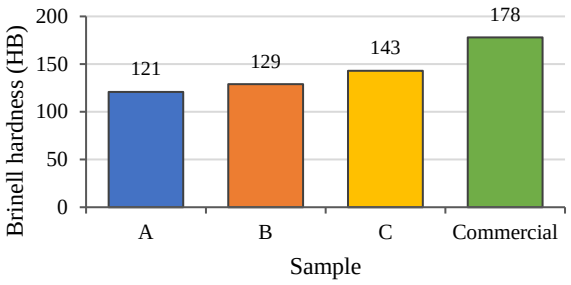

Fig. 8. Brinell hardness measured under a 9.8 kN load with a 10 mm ball indenter. The commercial reference is harder than all three developed formulations.

3.5 Wear Rate

Wear rate determines service life and is among the most consequential properties for a friction material. Table 5 and Figure 9 give the gravimetric results, with the underlying mass-loss data in Figure 10.

Sample A recorded 0.273 g/min, the lowest of the three and 66% below the 0.80 g/min commercial reference. Sample C followed at 0.413 g/min and Sample B was highest at 0.600 g/min, 2.2 times the wear of Sample A. All three developed linings wore more slowly than the commercial reference.

Wear does not follow hardness. Sample C is the hardest formulation yet wears 51% faster than the softest, and Sample B is intermediate in hardness but worst in wear. Across the series the hardness–wear correlation is weak and positive ($r = 0.28$, $n = 3$), the opposite sign to the inverse relation expected if indentation resistance governed wear. The low wear of Sample A is instead consistent with better interfacial bonding and more uniform reinforcement distribution, retaining particles in the matrix rather than allowing them to be liberated, although no microstructural evidence was obtained to confirm this. The rates are reported as a comparison within the present series.

TABLE 5: WEAR RATE RESULTS

Sample	W_1 (g)	W_2 (g)	$\dot{W}$ (g/min)
Sample A	34.51	33.69	0.273
Sample B	52.72	50.92	0.600
Sample C	32.86	31.62	0.413
Commercial	48	45.6	0.80

Test interval t = 3 min.

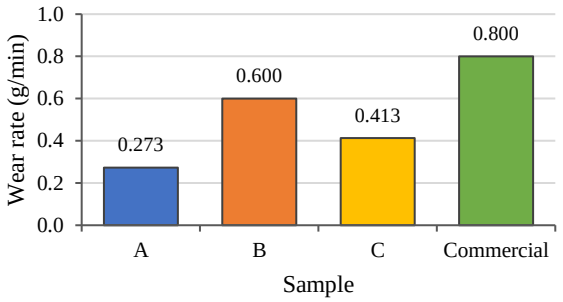

Fig. 9. Gravimetric wear rate over the 3 min test interval. Values are comparative within the present test series.

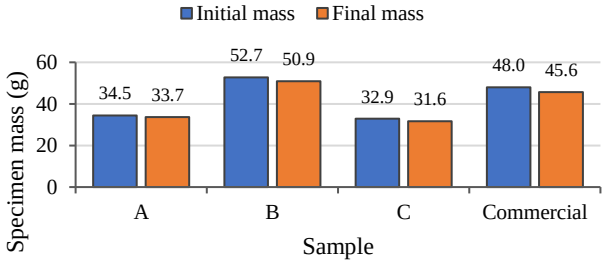

Fig. 10. Initial and final specimen mass over the 3 min wear test interval.

3.6 Compressive Strength

Brake linings carry high normal forces during braking, so ultimate compressive strength and deformation behaviour determine resistance to structural failure. Table 6 and Figure 11 give the results of two replicate runs per formulation.

Sample A attained the highest mean peak stress at 116.204 ± 0.755 N/mm² (mean ± SD, n = 2), Sample B 114.000 ± 0.004 N/mm² and Sample C 112.561 ± 0.490 N/mm², a 3.1% reduction from A to C. One-way analysis of variance across the six compression runs returns $F(2, 3) = 24.93$, $p = 0.014$, so the differences between formulations are statistically significant at $\alpha = 0.05$. Fisher's least significant difference at that level is 1.65 N/mm²: Sample A is separated from both B (difference 2.20 N/mm²) and C (3.64 N/mm²), whereas B and C are not separated from each other (1.44 N/mm²).

Two compositional factors are consistent with Sample A's advantage. Its metal powder content of 20 wt% is double that of B and C, and the metal particles act as load-bearing inclusions that fill voids in the polymer matrix. Its porosity is also the lowest at 14.29%, so applied force distributes across a larger solid cross-section rather than concentrating around voids.

Sample C combines the highest fibre loading with the lowest binder fraction at 45 wt%, giving the lowest binder-to-reinforcement ratio in the series at 1.29. With less resin available to coat each fibre, agglomeration and

© 2026 The Author(s). Published by Faculty of Engineering, Federal University Oye-Ekiti.
This is an open access article under the CC BY NC license. (https://creativecommons.org/licenses/by-nc/4.0/)

air entrapment would be expected, and the resulting weaker interfaces would reduce load transfer under compression. Sample C also records the highest water absorption at 2.22%, which is consistent with that interpretation. The interpretation is not established by these data, however: metal powder content also differs between A and the other two formulations, and no microstructural evidence was obtained. The effect on strength is in any case modest, at 3.1% across a 50% increase in fibre loading, and is expressed far more strongly in moisture uptake and wear.

TABLE 6: ULTIMATE COMPRESSIVE STRENGTH (N/MM²)

Sample	Run 1	Run 2	Mean
Sample A	115.670	116.738	116.204
Sample B	114.002	113.997	114.000
Sample C	112.214	112.907	112.561

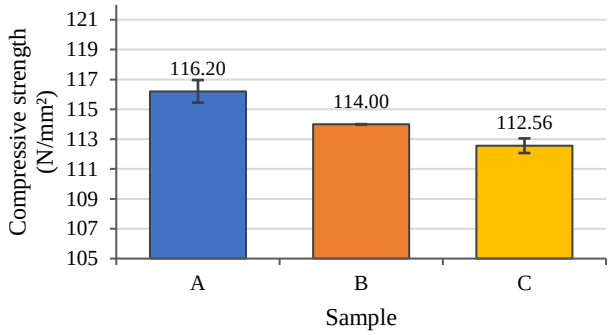

Fig. 11. Mean ultimate compressive strength of the three formulations; error bars show ± 1 standard deviation of the two replicate runs. One-way analysis of variance across the six runs gives F(2, 3) = 24.93, p = 0.014.

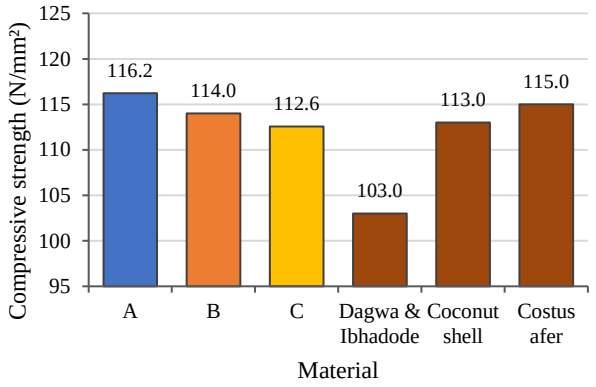

Fig. 12. Compressive strength of the three formulations against published asbestos-free linings.

Set against published asbestos-free linings, all three formulations perform well. Reported compressive strengths for comparable materials are 103 MPa for the experimental pad of Dagwa and Ibhadode (2006), 113 N/mm² for coconut shell composites (Ocheri et al., 2024) and 115 MPa for Costus afer (Ngwaba & Aikhuele, 2023). The present values of 112.6–116.2 N/mm² meet or exceed all three, with Sample A above every published figure and Sample C marginally below the highest of them (Fig. 12). No published specification limit for drum lining compressive strength was available for comparison, so these developed materials are benchmarked against demonstrated asbestos-free performance rather than against a standard.

3.7 IMPACT ENERGY

Impact strength indicates the ability of a lining to withstand the sudden shock loads produced by vibration and abrupt braking in service. Table 7 and Figure 13 give the results.

Sample B absorbed the most energy at 5.12 J, followed by Sample C at 4.85 J and Sample A at 4.39 J. All three exceed the commercial reference, Sample B by 43%. Higher absorbed energy is consistent with effective bonding between reinforcement and binder matrix, which distributes impact energy through the material rather than concentrating it at a crack front, although the ordering is reported as a comparison between the materials tested here.

TABLE 7: IMPACT TEST RESULTS

Sample	Impact energy (J)	vs. commercial
Sample A	4.39	+22.6%
Sample B	5.12	+43.0%
Sample C	4.85	+35.5%

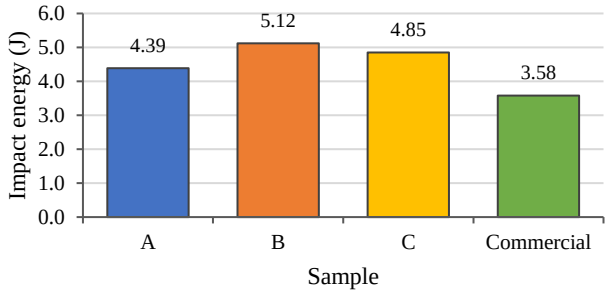

Fig. 13. Impact energy absorbed to fracture. All three developed linings exceed the commercial reference.

3.8 PROPERTY INTERACTIONS

Hardness rises and compressive strength falls across the series, while wear rate and water absorption are both lowest at Sample A. The strongest pairwise association is between hardness and compressive strength ($r = -0.962$), but with three formulations this coefficient carries one degree of freedom and does not reach significance ($p = 0.176$); the same applies to the association between fibre content and compressive strength ($r = -0.993$, $p = 0.077$) and between fibre content and water absorption ($r = +0.948$, $p = 0.207$). Weaker associations are found between porosity and water absorption ($r = +0.584$, $p = 0.603$) and between porosity and compressive strength ($r = -0.407$, $p = 0.733$), indicating that the mechanical response is not governed by pore fraction alone. None of the correlations computed here is statistically significant, and all are reported as descriptions of ordering across three formulations rather than as established relationships. The strength range across the series is in any case only 3.6 N/mm².

Compressive strength orders with binder and metal powder content as well as with fibre content. Sample A carries both the highest binder-to-reinforcement ratio (2.00) and twice the metal powder of the other two formulations, and these two factors cannot be separated from each other or from fibre loading in the present design.

Applying equation (8) to the seven measured properties, Sample A returns the highest composite desirability at D = 0.571, followed by Sample C at 0.454 and Sample B at 0.424. The normalised profile in Fig. 14 shows that Sample

© 2026 The Author(s). Published by Faculty of Engineering, Federal University Oye-Ekiti.
This is an open access article under the CC BY NC license. (https://creativecommons.org/licenses/by-nc/4.0/)

http://.doi.org/10.46792/fuoyejet.v11i3.1633 engineering.fuoye.edu.ng/journal

A leads on four of the seven properties and trails on three. The margin between Samples A and C is narrow and rests on wear rate, moisture uptake and compressive strength rather than on a sweep of the property set, so the ranking should be read as an ordering of candidates for further testing rather than as a decisive separation.

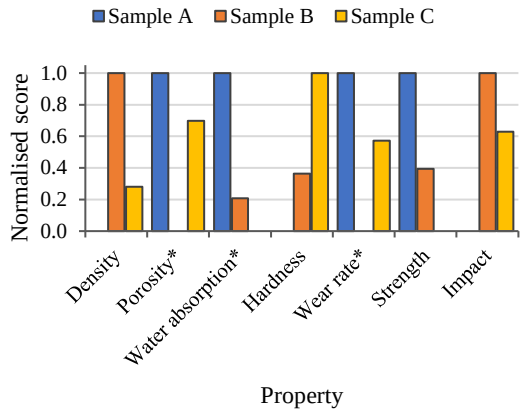

Fig. 14. Normalised property profile of the three formulations. Porosity, water absorption and wear rate are inverted so that a higher score is better throughout; a score of zero denotes the poorest of the three formulations on that property.

4 Discussion

4.1 Binder Starvation as a Proposed Mechanism

The most consistent pattern in the data is the inverse ordering of hardness and compressive strength ($r = -0.962$, $p = 0.176$). With three formulations this is a description of ordering and not a demonstrated relationship. What follows proposes a mechanism consistent with that ordering; it does not establish one, and no microstructural evidence was obtained in this work that would allow it to be tested directly.

Hardness probes only the near-surface response. As ceramic loading rises the indenter encounters a greater area fraction of hard mineral, so the reading climbs from 121 to 143 HB. Compressive strength depends instead on load transfer through the fibre–matrix interface, which requires each fibre to be wetted by resin. If the available binder is insufficient to coat the total fibre surface area, unwetted fibres would be expected to agglomerate, entrap air and form weaker interfaces that reduce load transfer. This is the binder starvation mechanism, and it is advanced here as a hypothesis.

Three observations in the present data are consistent with that hypothesis, although none is decisive and they are not independent of one another. First, Sample C combines the highest fibre loading with the lowest binder fraction and returns simultaneously the highest hardness and the lowest strength. Second, water absorption tracks the same ordering, rising from 0.44% to 2.22% across the series, which is what an increasingly interconnected void network would produce. Third, wear rate does not follow hardness ($r = +0.281$, $p = 0.819$), which would be expected if hard particles were inadequately bonded and liberated rather than retained. A competing explanation cannot be excluded on these data: metal powder falls from 20 wt% in Sample A to 10 wt% in B and C, and the loss of load-bearing metallic inclusions would depress strength and raise void content in the same direction. The present design cannot discriminate between the two.

The magnitude of the effect differs sharply between properties, and this is itself informative. Compressive strength falls by only 3.1% across a 50% increase in fibre loading, whereas moisture uptake rises approximately fivefold and wear rate 2.2-fold. Whatever mechanism operates over this range therefore acts on the interface and the pore network well before it measurably degrades bulk load-bearing capacity, and moisture uptake is the more sensitive indicator of the transition than compressive strength is.

If binder starvation is the operative mechanism, the threshold in this material system would lie near 20–25 wt% ceramic fibre at 50 wt% phenolic binder, corresponding to a binder-to-reinforcement ratio between 1.67 and 2.00. This is consistent with published work on fibre-reinforced friction composites, in which properties improve with reinforcement content only until the binder available to wet the reinforcement becomes insufficient (Ammar et al., 2023), and with the agglomeration reported in stir-cast composites above 15 wt% reinforcement (Ambali et al., 2023). Confirmation would require scanning electron microscopy of fracture and worn surfaces to establish whether unwetted fibre bundles and interfacial debonding are present, together with a formulation series in which binder fraction is varied independently of fibre content. Until that evidence exists, the practical implication can be put no more strongly than this: the binder-to-reinforcement ratio, rather than reinforcement content considered alone, is the formulation variable worth controlling, and hardness alone is a misleading selection criterion for friction materials.

4.2 Comparison with Published Asbestos-Free Linings

Hardness is competitive against published work but not against the commercial reference. At 121–143 HB the developed linings exceed the 103 HB reported for a Costus afer composite (Ngwaba & Aikhuele, 2023) and the 92 HB reported for an asbestos-free experimental pad by Dagwa and Ibhadode (2006), but fall 20–32% below the commercial lining at 178 HB, which indicates a higher abrasive or metallic content in the reference material. Apparent porosity at 14.29–17.14% is below the commercial reference throughout. Bulk density at 1.29–1.54 g/cm³ is comparable to the 1.30 g/cm³ of the Costus afer composite (Ngwaba & Aikhuele, 2023) but below the 1.65 specific gravity reported by Dagwa and Ibhadode (2006), the 1.91 of coconut shell linings (Ocheri et al., 2024) and the commercial reference, despite the ceramic and metallic constituents, which points to incomplete consolidation rather than to the formulation.

Compressive strength at 112.56–116.20 N/mm² sits at or above every published asbestos-free value available for comparison: 103 MPa for the experimental pad of Dagwa and Ibhadode (2006), 113 MPa for coconut shell (Ocheri et al., 2024) and 115 MPa for Costus afer (Ngwaba & Aikhuele, 2023), as Fig. 12 shows. All three formulations therefore meet or exceed the strength demonstrated by published asbestos-free linings, which is the most directly relevant benchmark available in the absence of a published specification limit. Water absorption at 0.44–2.22% is of the same order as the 1.2% reported by Ngwaba and Aikhuele (2023), with Sample A well inside that figure and Samples B and C above it. Bulk density is

© 2026 The Author(s). Published by Faculty of Engineering, Federal University Oye-Ekiti.
This is an open access article under the CC BY NC license. (https://creativecommons.org/licenses/by-nc/4.0/)

http://.doi.org/10.46792/fuoyejet.v11i3.1633 engineering.fuoye.edu.ng/journal

the single property on which all three formulations fall short of both the published values and the commercial reference, and the discussion below attributes this to the consolidation achieved rather than the compositions themselves.

TABLE 8: PRESENT RESULTS AGAINST PUBLISHED VALUES

Property	This work	Literature
Density (g/cm³)	1.29–1.54	1.30–1.91
Porosity (%)	14.3–17.1	–
Water abs. (%)	0.44–2.22	1.2
Hardness (HB)	121–143	92–103
UCS (MPa)	112.6–116.2	103–115
Impact (J)	4.39–5.12	–

4.3 CONSOLIDATION AND PROCESS EFFECTS

Bulk density and apparent porosity together characterise the degree of consolidation achieved during moulding. Moulding pressure is the dominant determinant of porosity and density in friction composites (Ammar et al., 2023; Dagwa & Ibhadode, 2006). At 1.29–1.54 g/cm³ the developed linings sit below the commercial reference while their open porosity is only 14–17%, indicating that a proportion of the void volume is closed rather than interconnected. Raising the degree of consolidation, through higher compaction pressure and a longer dwell before gelation of the binder, is therefore the most direct route to increased bulk density in this material system, and it is independent of the formulation variables examined here.

Replicate spread varied across the series, as is characteristic of a hand-blended composite produced in a single campaign. With two specimens per formulation, the analysis of variance is read here as confirming the ordering of the three formulations rather than as a precise estimate of the magnitude of the differences between them. The consequence for interpretation is specific. Bulk density and apparent porosity characterise the process at least as much as the formulation, and are read accordingly. The relative ordering between formulations, which is the subject of this paper, is unaffected, because all three were produced under identical conditions. Reproducing the absolute values in another laboratory would require the compaction pressure to be monitored at the charge.

4.4 SCOPE OF THE PRESENT FINDINGS

Five considerations define the scope of what the present data establish, and they set the agenda for the work that follows.

1. The formulation series varies binder fraction and metal powder content alongside ceramic fibre, so the reported property changes characterise the three formulations as prepared. Isolating the contribution of ceramic fibre requires a series in which the remaining constituents are held constant.

2. Replication was carried out for compressive strength. The remaining six properties were determined once per material, and the differences between formulations in those properties are reported as an ordering; extending replication across the full property set would allow each ordering to be tested formally.

3. The binder starvation mechanism is advanced on the consistency of several indirect indicators. Scanning electron microscopy of fracture and worn surfaces would establish it directly, by revealing whether unwetted fibre bundles and interfacial debonding are present at the higher reinforcement loadings.

4. Wear was measured gravimetrically under a single fixed set of conditions, and the resulting rates rank the materials tested here. Conversion to specific wear rate, and comparison with published values, requires testing under a normalised procedure such as SAE J661. Hardness was measured under an ASTM E10 condition intended for metals and likewise ranks materials indented identically.

5. Thermal and friction characterisation falls outside the present programme. Friction coefficient, fade behaviour, thermal conductivity and elevated-temperature strength determine performance in service, and establishing them for these formulations is the substance of the qualification programme set out in the conclusions.

4.5 SELECTION OF THE PREFERRED FORMULATION

Sample A is identified as the preferred of the three formulations for tricycle drum service on the evidence available. It leads on four of seven properties: lowest apparent porosity, lowest water absorption, lowest wear rate and highest compressive strength. Its composite desirability of 0.571 exceeds Sample C at 0.454 and Sample B at 0.424. The margins are narrow, and the selection rests on the properties most directly relevant to drum service, wear resistance, moisture uptake and compressive strength, rather than on a sweep of the property set.

Three properties favour the other formulations. Sample A records the lowest hardness of the three at 121 HB, below the commercial reference; the lowest impact energy at 4.39 J, though still 23% above the commercial reference; and the lowest bulk density at 1.29 g/cm³, which the foregoing analysis attributes to consolidation rather than to composition. The advantage of Sample A cannot be assigned to any single constituent. It carries the highest binder-to-reinforcement ratio in the series at 2.00 and twice the metal powder of the other two formulations, and these differences act together. Sample A is accordingly identified as the formulation to carry forward into tribological and thermal qualification, in which friction coefficient, fade behaviour and elevated-temperature performance will determine its suitability for service.

4.6 PRACTICAL IMPLICATIONS

The route described here uses constituents obtainable in Nigeria and equipment found in polytechnic and small workshop settings. Eliminating asbestos removes the occupational and public health burden associated with it, and local production offers a route to reducing dependence both on imported linings of variable quality and on counterfeit substitutes that may still contain asbestos.

One process intervention supports that potential directly. Compaction at a pressure monitored at the charge is the single change most likely to raise bulk density and make the route reproducible at scale; it requires instrumentation but no reformulation. The qualification programme set out in the conclusions establishes the performance basis for production.

5 CONCLUSIONS

Three asbestos-free ceramic–glass fibre reinforced

© 2026 The Author(s). Published by Faculty of Engineering, Federal University Oye-Ekiti.
This is an open access article under the CC BY NC license. (https://creativecommons.org/licenses/by-nc/4.0/)

http://.doi.org/10.46792/fuoyejet.v11i3.1633 engineering.fuoye.edu.ng/journal

phenolic brake linings for tricycle drum braking systems were developed by compression moulding and characterised across seven physical and mechanical properties against a commercial reference. Because binder and metallic filler fractions varied alongside ceramic fibre content, the findings below describe three candidate formulations and do not isolate the effect of ceramic fibre loading.

1. Sample A, at 20 wt% ceramic fibre and 20 wt% metal powder, returned the best overall profile of the three. It gave the lowest apparent porosity (14.29%), lowest water absorption (0.44%), lowest wear rate (0.273 g/min) and highest compressive strength (116.204 N/mm²), with a composite desirability of 0.571 against 0.454 and 0.424 for Samples C and B. One-way analysis of variance on the compression data confirms that Sample A is separated from both other formulations, $F(2, 3) = 24.93$, $p = 0.014$.

2. Hardness rose from 121 to 143 HB across the series while compressive strength fell from 116.204 to 112.561 N/mm². Binder starvation at the higher reinforcement loadings is proposed as the mechanism most consistent with this ordering, and microstructural examination is required to establish it directly. The strength effect is small at 3.1%, whereas moisture uptake rises approximately fivefold and wear rate 2.2-fold over the same range, so the mechanism is expressed principally in the interface and pore network rather than in bulk load-bearing capacity.

3. All three linings exceeded the commercial reference in impact energy by 23–43%, and all were less porous, absorbed less moisture and wore more slowly than the reference in the tests performed. All three were softer: the commercial lining measured 178 HB against 121–143 HB for the developed formulations.

4. Compressive strength of 112.6–116.2 MPa meets or exceeds every published asbestos-free value available for comparison, from 103 MPa (Dagwa & Ibhadode, 2006) to 115 MPa (Ngwaba & Aikhuele, 2023); water absorption of 0.44–2.22% is of the same order as published values; and apparent porosity is below the commercial reference throughout. Bulk density is the exception: at 1.29–1.54 g/cm³ all three formulations sit below both the commercial reference and the published range, which together with the implied closed-void fraction identifies consolidation, rather than composition, as the property to address.

Tribological, thermal and microstructural characterisation constitutes the next stage of this work, and is required before commercial production or field deployment of any of these formulations. Further work should proceed in the following order: fabrication with the compaction pressure monitored at the charge, to raise bulk density and establish reproducibility; a formulation series that isolates ceramic fibre content with binder and metallic filler held constant, with replication across the full property set; scanning electron microscopy of fracture and worn surfaces to establish the proposed binder starvation mechanism directly; thermal characterisation by thermogravimetric analysis, thermal conductivity measurement and elevated-temperature strength testing, which will establish the thermal rationale for ceramic fibre in this material system; intermediate fibre loadings between 15 and 25 wt% to locate the threshold precisely; friction and fade characterisation under SAE J661 and SAE J2522; and on-vehicle trials under representative Nigerian tricycle duty cycles.

ACKNOWLEDGMENT

The authors have reviewed this and accept the content of this research work.

REFERENCES

Adeniyi, P. A., Ishola, A. O., Laoye, B. J., Olatunji, B. P., Bankole, O. O., Shallie, P. D., & Ogundele, O. M. (2016). Neural and behavioural changes in male periadolescent mice after prolonged nicotine-MDMA treatment. *Metabolic brain disease, 31*(1), 93-107.

Balogun, V. A., Aramcharoen, A., Mativenga, P. T., & Chuan, S. K. (2013). Impact of Machine Tools on the Direct Energy and Associated Carbon Emissions for a Standardized NC Toolpath *Re-engineering Manufacturing for Sustainability* (pp. 197-202): Springer.

Balogun, V. A., Kirkwood, N. D., & Mativenga, P. T. (2014). Direct Electrical Energy Demand in Fused Deposition Modelling. *Procedia CIRP, 15*, 38-43.

Balogun, V. A., & Mativenga, P. T. (2013). Modelling of direct energy requirements in mechanical machining processes. *Journal of Cleaner Production, 41*, 179-186.

Chen, L., Hoey, J., Nugent, C. D., Cook, D. J., & Yu, Z. (2012). Sensor-based activity recognition. *IEEE Transactions on Systems, Man, and Cybernetics, Part C (Applications and Reviews), 42*(6), 790-808.

Kong, D., Choi, S., Yasui, Y., Pavanaskar, S., Dornfeld, D., & Wright, P. (2011). Software-based tool path evaluation for environmental sustainability. *Journal of Manufacturing Systems, 30*(4), 241-247. doi: 10.1016/j.jmsy.2011.08.005

Young, J., Roy, H. S., & Young, J. (2007). Transforming server-side processing grammars: Google Patents

Adetunji, O. R., Adedayo, A. M., Ismailia, S. O., Dairo, O. U., Okediran, I. K., & Adesusi, O. M. (2022). Effect of silica on the mechanical properties of palm kernel shell based automotive brake pad. Mechanical Engineering for Society and Industry, 2(1), 7–16. https://doi.org/10.31603/mesi.6178

Ambali, A. O., Oyelaran, O. A., Bolaji, B. O., & Abdulmalik, I. O. (2022). Processing methods and properties of aluminium-SiCp metal matrix composites produced by stir casting for marine applications: A review. FUOYE Journal of Engineering and Technology, 7(4), 465–473. https://doi.org/10.46792/fuoyejet.v7i4.860

Ambali, A. O., Oyelaran, O. A., Bolaji, B. O., Abdulrahman, J., Suleiman, O. A., & Araromi, O. T. (2023). Morphology of Al-2.5%Mg/xSiCp composite developed by stir casting process. FUOYE Journal of Engineering and Technology, 8(3), 336–342. https://doi.org/10.46792/fuoyejet.v8i3.1061

Ammar, Z., Ibrahim, H., Adly, M., Sarris, I., & Mehanny, S. (2023). Influence of natural fiber content on the frictional material of brake pads: A review. Journal of Composites Science, 7(2), 72. https://doi.org/10.3390/jcs7020072

Asafa, T. B., Olawuni, E. O., & Durowoju, M. O. (2020). Hardness and elastic modulus of Al-based composite developed from aluminium piston scraps using alumina and snail shell as reinforcements. FUOYE Journal of Engineering and Technology, 5(2), 147–150. https://doi.org/10.46792/fuoyejet.v5i2.531

ASTM International. (2018a). ASTM D570-98(2018): Standard test method for water absorption of plastics. ASTM International.

ASTM International. (2018b). ASTM E10-18: Standard test method for Brinell hardness of metallic materials. ASTM International.

Bashir, M., Qayoum, A., & Saleem, S. S. (2019). Influence of lignocellulosic banana fiber on the thermal stability of brake pad material. Materials Research Express, 6(11), 115551. https://doi.org/10.1088/2053-1591/ab37bd

Bijwe, J. (1997). Composites as friction materials: Recent developments in non-asbestos fiber reinforced friction materials. A review. Polymer Composites, 18(3), 378–396. https://doi.org/10.1002/pc.10289

Dagwa, I. M., & Ibhadode, A. O. A. (2006). Some physical and

© 2026 The Author(s). Published by Faculty of Engineering, Federal University Oye-Ekiti.
This is an open access article under the CC BY NC license. (https://creativecommons.org/licenses/by-nc/4.0/)

mechanical properties of asbestos-free experimental brake pad. Journal of Raw Materials Research, 3(1), 1–10. https://doi.org/10.83043/jmynaq42

Federal Road Safety Corps. (2021). Road traffic crash report. Federal Road Safety Corps.

Hee, K. W., & Filip, P. (2005). Performance of ceramic enhanced phenolic matrix brake lining materials for automotive brake linings. Wear, 259(7–12), 1088–1096. https://doi.org/10.1016/j.wear.2005.02.083

Ibhadode, A. O. A., & Dagwa, I. M. (2008). Development of asbestos-free friction lining material from palm kernel shell. Journal of the Brazilian Society of Mechanical Sciences and Engineering, 30(2), 166–173. https://doi.org/10.1590/S1678-58782008000200010

Idris, U. D., Aigbodion, V. S., Abubakar, I. J., & Nwoye, C. I. (2015). Eco-friendly asbestos free brake-pad: Using banana peels. Journal of King Saud University - Engineering Sciences, 27(2), 185–192. https://doi.org/10.1016/j.jksues.2013.06.006

Ikpambese, K. K., Gundu, D. T., & Tuleun, L. T. (2016). Evaluation of palm kernel fibers (PKFs) for production of asbestos-free automotive brake pads. Journal of King Saud University - Engineering Sciences, 28(1), 110–118. https://doi.org/10.1016/j.jksues.2014.02.001

International Agency for Research on Cancer. (2012). Arsenic, metals, fibres, and dusts (IARC Monographs on the Evaluation of Carcinogenic Risks to Humans, Vol. 100C). International Agency for Research on Cancer.

Jang, H., Ko, K., Kim, S. J., Basch, R. H., & Fash, J. W. (2004). The effect of metal fibers on the friction performance of automotive brake friction materials. Wear, 256(3–4), 406–414. https://doi.org/10.1016/S0043-1648(03)00445-9

Kumar, V. V., & Kumaran, S. S. (2019). Friction material composite: Types of brake friction material formulations and effects of various ingredients on brake performance. A review. Materials Research Express, 6(8), 082005. https://doi.org/10.1088/2053-1591/ab2404

Mutlu, I., Eldogan, O., & Findik, F. (2005). Production of ceramic additive automotive brake lining and investigation of its braking characterisation. Industrial Lubrication and Tribology, 57(2), 84–92. https://doi.org/10.1108/00368790510583401

Ngwaba, L. C., & Aikhuele, D. O. (2023). Development and evaluation of asbestos-free brake pads produced from Costus afer waste and local gum Arabic. Journal of Mechanical Engineering and Technology, 15(1), 11–24. https://doi.org/10.54554/jmet.2023.15.01.002

Ocheri, C., Mbah, C. N., & Alabi, O. O. (2024). Development and characterization of asbestos free brake pad using coconut shell as a base material. Journal of Metallurgy and Materials Engineering, 10(1), 1–8. https://jmme.nigerianmetsociety.org/index.php/home/article/view/3

SAE International. (2014). SAE J2522: Dynamometer global brake effectiveness. SAE International.

SAE International. (2021). SAE J661: Brake lining quality test procedure. SAE International.

Singh, T., Pruncu, C. I., Gangil, B., Singh, V., & Fekete, G. (2020). Comparative performance assessment of pineapple and Kevlar fibers based friction composites. Journal of Materials Research and Technology, 9(2), 1491–1499. https://doi.org/10.1016/j.jmrt.2019.11.074

Thiyagarajan, V., Kalaichelvan, K., Vijay, R., & Singaravelu, D. L. (2016). Influence of thermal conductivity and thermal stability on the fade and recovery characteristics of non-asbestos semi-metallic disc brake pad. Journal of the Brazilian Society of Mechanical Sciences and Engineering, 38(4), 1207–1219. https://doi.org/10.1007/s40430-015-0448-8

© 2026 The Author(s). Published by Faculty of Engineering, Federal University Oye-Ekiti.
This is an open access article under the CC BY NC license. (https://creativecommons.org/licenses/by-nc/4.0/)